Original Article

DOI: 10.5582/bst.2024.01097

Suppression of STK39 weakens the MASLD/MASH process by protecting the intestinal barrier

Qing Xu[1,§], Fei Liu[2,§], Zhenru Wu[1], Menglin Chen[1], Yongjie Zhou[3,*], Yujun Shi[1,3,*]

[1] Institute of Clinical Pathology & Department of Pathology, Key Laboratory of Transplant Engineering and Immunology, NHC, West China Hospital, Sichuan University, Chengdu, China;
[2] Department of Biliary Surgery, West China Hospital, Sichuan University, Chengdu, China;
[3] Laboratory of Liver Transplantation, West China Hospital, Sichuan University, Chengdu, China.

SUMMARY STK39 is reportedly a critical negative regulator of intestinal barrier. Pharmacological targeting of STK39 is expected to protect the intestinal barrier and thereby weaken metabolic dysfunction-associated steatohepatitis (MASH); Proximal colon biopsy tissues from patients with metabolic dysfunction-associated steatotic liver disease (MASLD) and those without MASLD were analyzed for STK39 expression. Wildtype (WT) mice and systemic STK39 gene knockout ($STK39^{-/-}$) male mice were fed a normal diet or a high-fat methionine-choline deficient diet (HFMCD) for 8 weeks. The MASH mice were grouped and treated with ZT-1a (a STK39 inhibitor) or vehicle intraperitoneal injection during the procedure of HFMCD induction. Liver and intestinal tissues were collected for further examination; Colon tissues from patients with MASLD exhibited higher levels of STK39 than those from subjects without MASLD. Knockout of STK39 diminished $CD68^{+}$ Kupffer cells and α-SMA^{+} hepatic stellate cells infiltration in mouse MASH model. Treatment with ZT-1a also prevented severe steatohepatitis in a mouse MASH model, including milder histological and pathological manifestations (lobular inflammation and fibrosis) in the liver. Interestingly, Inhibition of STK39 had minimal effects on hepatic lipid metabolism. The reduced liver injury observed in mice with STK39 inhibition was linked to significant decreases in mucosal inflammation, tight junction disruption and intestinal epithelial permeability to bacterial endotoxins; Collectively, we have revealed that inhibiting STK39 prevents the progression of MASH by protecting the intestinal epithelial barrier.

Keywords STK39, ZT-1a, MASLD/MASH, intestinal barrier

1. Introduction

Globally, nonalcoholic fatty liver disease (MASLD) and nonalcoholic steatohepatitis (MASH), both diet-related, are among the most prevalent causes of chronic liver disease (*1*). It is estimated that 20% of MASLD patients develop MASH, and 15% MASH patients progress to cirrhosis (*2*). Despite the fact that most MASLD/MASH patients remain asymptomatic, they face an elevated risk of developing hepatocellular carcinoma (*3*). This poses a considerable hindrance to the development of therapeutic strategies and biomarkers for advanced MASH.

The possible involvement of impaired intestinal epithelial permeability in the pathogenesis of MASH has been emphasized by several recent studies (*4-7*). The intestinal barrier severs as a protective shield against potentially harmful metabolites, bacteria, and their antigens. Consequently, immunologic regulation of the commensal microbiota and the intestinal barrier is crucial and has been preserved throughout evolution (*8*). Elevated intestinal epithelial permeability is associated with increased serum endotoxin levels, a powerful inducer of hepatic inflammation, in both human and animal models (*9*). In recent years, diet, particularly a high-fat diet (HFD), has emerged as one of the most significant factors affecting the function of the intestinal epithelial barrier and leading to endotoxemia in healthy individuals (*10*). Moreover, human MASH and MASH-related cirrhosis often exhibit increased intestinal epithelial permeability and small intestinal bacterial overgrowth (*7*). However, it remains unclear whether the persistent systemic inflammation observed in MASH patients is a consequence or a contributing factor to intestinal epithelial barrier dysfunction.

The tight junctions (TJs) of intestinal epithelium cells form a crucial component of the intestinal barrier (*11*). The physiological functions of the TJ proteins are sustained by three essential proteins: zonula occludens-1

(ZO-1), Occludin, and claudins (*12*). Damage to the TJs barrier due to high-fat diet contributes to the progression of MASLD/MASH. A human study revealed that patients with MASLD exhibit increased gut epithelial permeability, decreased levels of tight junction proteins (such as ZO-1, claudin 1, and Occludin), and elevated inflammation levels; these alterations are closely linked to the occurrence and progression of MASLD (*13*). A meta-analysis indicated that, compared to healthy volunteers, patients with MASLD and MASH are more prone to having enhanced intestinal permeability (*14*). The increased gut permeability heightens the liver's exposure to intestine-derived bacterial products (such as LPS, short-chain fatty acids, bile acids, cytokines, and ethanol), which exacerbate hepatic inflammation and fibrosis by activating toll-like receptor (TLR) signaling and the inflammasome (*15,16*). Therefore, it is necessary and particularly crucial to prevent MASLD/MASH by maintaining TJs function. TJ proteins, the most important intercellular junctions of intestinal epithelial cells (IECs), seal the paracellular space between adjacent IECs (*17*). TJ proteins regulate the transport of water, ions, and solutes through the paracellular pathway and prevent the passage of immunogenic macromolecules, particularly gut bacterial metabolites (*18*). Previous research has shown that upregulation of ZO-1 and Occludin can inhibit the increase in intestinal permeability and attenuate MASLD (*19*). Therefore, drugs that prevent TJ protein disruption are widely considered an effective approach for MASLD/MASH therapies.

Serine/threonine kinase 39 (STK39), a member of MAP4K family, comprises an N-terminal series of proline/alanine repeats (PAPA box), followed by a catalytic domain, a nuclear localization signal, a potential caspase cleavage motif, and a C-terminal regulatory region. STK39 is present in both the nucleus and the cytoplasm (*20*). Recent studies have demonstrated that STK39 knockout mice exhibit a significant increase in intestinal transepithelial resistance, a marked decrease in paracellular permeability to fluorescent isothiocyanate dextran, and altered sodium ion selectivity at apical tight junctions (*21*). Furthermore, overexpression of STK39 impairs the intestinal barrier and enhances the permeability of the intestinal epithelium (*22*). Therefore, it is highly likely that STK39 is involved in the progression of MASH through the intestinal barrier. 5-chloro-N-(5-chloro-4-((4-chlorophenyl)(cyano) methyl)-2-methylphenyl)-2-hydroxybenzamide (ZT-1a) is a potent, non-ATP-competitive, and selective STK39 inhibitor (*23*). ZT-1a has previously been shown to be neuroprotective in murine ischemic stroke models (*24*). However, whether ZT-1a could be used to protect the intestinal barrier and thereby mitigate MASH remains unknown.

In this study, we systematically investigated the impact of STK39 inhibitors on the pathogenesis of MASH. STK39 was overexpressed in colon tissues from MASH patients and mice. In the HFMCD-induced MASH mouse model, ZT-1a exhibited attenuated liver inflammation and liver cirrhosis, without changes in liver lipid accumulation. This may be partly due to reduced intestinal permeability and decreased LPS production. Furthermore, inhibiting STK39 reduced dextran sulfate sodium (DSS)-induced intestinal barrier damage and prevented LPS-induced hepatic inflammation or fibrosis. Here, our data support the idea that targeting STK39 may be a potent strategy to improve MASH.

2. Materials and Methods

2.1. Mice

STK39$^{-/-}$ mice were purchased from VIEWSOLID Ltd. All mice were housed at up to 5 mice per cage in specific-pathogen-free conditions under a 12 h light/dark cycle at constant temperature (22°C). The animals had free access to water and standard laboratory chow. Animal care and experimental procedures were conducted in accordance with national and international laws and policies and were approved by the Animal Care and Use Committee of Sichuan University (No. 2020455A). The animal study protocol was approved by the Ethics Committee of West China Hospital of 20230530005 and date of 2023.05.31.

2.2. Informed consent Statement

Informed consent was obtained from all subjects involved in the study. Written informed consent has been obtained from the patient(s) to publish this paper.

2.3. MASH diet

To establish MASH model, mice were subjected to HFMCD diet or HFD diet with 1% sulfate sodium (DSS). For HFMCD model, 6-8 weeks-old male WT mice and STK39$^{-/-}$ mice were fed a high fat (60 Kcal%), methionine (1%) without choline (HFMCD, A06071302, ReadyDietech) for 8 weeks. The normal diet was standard mouse chow containing 16% protein, 61% carbohydrate, and 7.2% fat. For HFD + 1% DSS model, mice were fed a high fat, high cholesterol (HFD), and 1% DSS for 4 weeks. The diet consisted of 0.2% cholesterol, 20% protein, 43% CHO2I, and 23% fat (6.6% trans-fat) (D09100310, ReadyDietech). Additionally, 1% DSS was provided in the drinking water. A normal diet was mentioned as above.

2.4. ZT-1a treatment

ZT-1a (HY-136532, MedChemExpress), a non-ATP-competitive, selective SPAK inhibitor that inhibits SPAK activity (*23*), was concomitantly administered weekly *via* intraperitoneal injection (100 mg/kg) to

mice during induction of MASH.

2.5. Lentivirus transduction

HepG2 and SW480 cell lines were seeded in a 6-well plate and cultured for 12-24 h to 20-30% confluence in complete medium before transfection. The culture medium was replaced with serum-free medium containing lentivirus (Weizhen; Shandong, China) and 5 μg/ml polybrene (Weizhen). As a negative control, cells were transduced with an empty vector. After incubating for 8-12 h, the serum-free medium was changed to complete medium. Transfection efficiency was observed under a fluorescence microscope at 48-72 h after infection. Then, cells were treated with 5 μg/ml puromycin (MCE) for 2 days to select stably transfected cells.

2.6. Histology

Excised liver tissues were fixed in 10% neutral buffer formalin and embedded in paraffin. Formalin-fixed liver tissue sections were stained with H&E or Sirius Red. A blinded pathologist performed histologic grading of the liver tissue sections using the MASH-CRN scoring system. Colons were embedded in Tissue-Tek OCT compound (Sakura Finetek USA, Inc, Torrance, CA) and flash-frozen in liquid nitrogen. Colonic cryosections were stained with H&E. Histology images were obtained using a Zeiss Light Microscope (Leica, Jena, Germany).

2.7. Immunohistochemistry and Immunofluorescence

Liver cryosections were fixed with 4% paraformaldehyde in phosphate-buffered saline, and blocked with 3% bovine serum albumin in phosphate-buffered saline. Colonic cryosections were fixed with acetone for 5 minutes at -20°C and blocked with 5% bovine serum albumin in phosphate-buffered saline. The following primary antibodies (dilutions 1:100) were used: F4/80 (70076, Cell Signaling Technology), CD68 (ER1901-32, Huabio), and STK39 (ab128894, Abcam) Both liver and colonic cryosections were incubated with primary antibodies overnight at 4°C. Slides were washed twice with PBS-T and incubated with Rabbit EnVision+ System-HRP (Dako) or Mouse EnVision+ System-HRP (Dako) at RT for 30 min. Sections were counterstained with Mayer's hematoxylin and dehydration was performed by incubation in 70% and 100% ethanol followed by xylene, before slides were mounted using Pertex (Histolab).

For immunofluorescence analysis, tissue samples were dissected, washed with ice-cold PBS, and then fixed with 4% PFA in PBS for 12 h at 4°C. The tissues were incubated in 30% sucrose (Sigma-Aldrich) overnight, embedded in optimal cutting temperature compound (Sakura Finetek, America), frozen on dry ice, and sectioned at -20°C. The frozen tissues were sectioned at a thickness of 4 μm on a cryostat (Leica). When applicable, sections were incubated in blocking buffer (5% milk powder in PBS-T) for 30 min at 25°C, and stained with primary antibodies directed against the following proteins: Occludin (1:200; R1510-33 Huabio) and ZO1 (1:200; ER41204, HuaBio), in blocking buffer overnight at 4°C. After washing in PBS-T, the slides were incubated for 2 h with the following secondary antibodies: goat anti-rabbit IgG (H+L) secondary antibody, and DAPI (Sigma-Aldrich) for 30 min at 25°C and washed in PBS-T. Tissues were mounted in VECTASHIELD HardSet Antifade Mounting Medium (Vector Labs) prior to sample acquisition on a Leica Dive confocal/multiphoton microscope or a Nikon A1R HD25 confocal microscope. Images were processed with ImageJ (National Institutes of Health; Bethesda, MD, USA).

2.8. Quantitative Reverse Transcription PCR

Total RNA was isolated from liver tissue using the RNeasy Mini Kit (Qiagen, Valencia, CA) according to the manufacturer's instructions. RNA (1 mg) was reverse-transcribed to complementary DNA using the Bio-Rad iScript complementary DNA synthesis kit (Bio-Rad, Hercules, CA). Quantitative reverse-transcription PCR was performed using gene-specific primer sets (Supplementary Table S1, *http://www.biosciencetrends.com/action/getSupplementalData.php?ID=205*) and IQ SYBR Green Supermix (Bio-Rad) on a Mastercycler ep realplex PCR instrument (Eppendorf, Hamburg, Germany). The reaction conditions were 95℃ for15 seconds, followed by 40 cycles of 95°C for 3 seconds,55°C for 15 seconds, and 72°C for 20 seconds. Relative expression was calculated using the DDCt method with GAPDH serving as the reference housekeeping gene. Expression of the respective genes was normalized to that of GAPDH rRNA, and the normalized data are presented as the fold change in gene expression compared with that of control mice fed a normal diet.

2.9. Western blot

Cellular proteins were extracted from c-Kit+ cells after various treatments, and a BCA Protein Assay Kit (Beyotime Technology; Shanghai, China) was used to quantify total protein. Homogenates containing 50 μg of protein per sample were mixed with 5× loading buffer and denatured at 95°C for 5 min. Proteins were separated *via* SDS-PAGE (Baihe; Chengdu, China) and transferred onto 0.45 μm PVDF membranes (Millipore). The membranes were blocked with 5% non-fat dried milk, which was diluted in TBST, at room temperature for 2 h and incubated overnight at 4°C with primary antibodies

diluted in the same blocking buffer. The following primary antibodies (dilutions 1:1000) were used: TGFβ1 (ER31210, Huabio), α-SMA (ET1607-53, Huabio), IL-6(ab233706, Abcam), IL-17(RT1326, Huabio), NF-κB (ET1603-12, Huabio) and GAPDH (ET1601-4, Huabio). After washing 3 times with TBST, membranes were incubated with HRP-conjugated secondary antibody for 1 h at RT. The membranes were visualized using the Gel Doc™ XR System (Bio-Rad).

2.10. Serum chemistry

ALT and AST levels in the serum were measured using aspartate aminotransferase and alanine transaminase activity assay kits (Sigma-Aldrich). Total serum cholesterol and triglyceride levels were measured on the CX7 chemistry autoanalyzer (Beckman Coulter Diagnostics, Miami, FL).

2.11. Cytokine analysis

The concentration of key inflammatory cytokines in the serum were quantified using the Milliplex Map Kit (EMD Millipore Corporation, Billerica, MA) on a Bio-Plex 200 System (Bio-Rad). For liver cytokine analysis, frozen liver tissue samples were homogenized in cell extraction buffer supplemented with 1 mmol/L phenylmethylsulfonyl fluoride and protease inhibitor cocktail (Life Technologies), and the supernatants were analyzed by multiplex enzyme-linked immunosorbent assay.

2.12. *In vivo* permeability assay

Intestinal permeability was assessed by *in vivo* FITC-dextran (FD4; Sigma-Aldrich) permeability assay as described previously17. Mice fasted for 4 h were gavaged with 0.6 mg/g body weight FITC-dextran (4 KDa) solution and blood was collected by submandibular bleeding after 3 h. Fluorescence intensity in the serum was measured using Fluorescence Spectrophotometer. FITC-dextran concentrations were determined from a standard curve generated by serial dilutions of FITC dextran.

2.13. Statistical analysis

Statistical differences were analyzed by unpaired Student's *t*-test analysis for multiple group comparison. A p value < 0.05 was considered statistically significant. Except for the human data, all animal experiments were repeated at least two times on two separate occasions.

3. Results

3.1. MASLD patients and MASH mice have enhanced STK39 expression in the colonic mucosa.

We initially explored the role of STK39 in colon tissues from MASLD. Biopsies taken from the proximal colon of six patients with MASLD and five subjects without MASLD (controls), who underwent surveillance colonoscopy, were examined for STK39 protein expression using immunochemistry. Individuals with elevated serum aspartate aminotransferase (AST) and alanine aminotransferase (ALT) levels, increased serum cholesterol and triglycerides, and hepatic steatosis confirmed by a right upper quadrant ultrasound (RUQ US) were diagnosed with MASLD (Figure1A-C). Due to the absence of liver biopsy specimens, we were unable to specifically identify patients with MASH. Therefore, we collectively referred to the study cohort as having MASLD. Subjects with a body mass index of less than 25 kg/m^2, normal serum AST levels (≤ 40 U/L), and a negative liver ultrasonography were defined as controls (Figure 1D). The intestinal mucosa tissue of MASLD patients exhibited noticeably increased STK39 protein levels, as shown in Figure 1E. Remarkably, higher intestinal mucosal STK39 expression was associated with more severe mucosal inflammation in MASLD patients, as evidenced by a greater infiltration of immune cells in the mucosa (Figure 1F). Interestingly, we discovered the Occuldin was also suppressed in colon tissues from MASLD patients (Figure 1G). Additionally, we examined STK39 expression in colon tissues from MASH model mice. Consistent with human observations, STK39 was upregulated in colon tissues from MASH mice (Figure 1H). We examined the hepatic stellate cell (HSCs) and Kupper cells infiltration in liver from mouse MASH model and control. we found the protein expression of α-SMA, a key marker of hepatic stellate cell (HSC) activation, was significantly upregulated in MASH mice (Figure 1I). And CD68 staining revealed increased infiltration of hepatic macrophages in MASH mice (Figure 1J). These results indicated more α-SMA$^+$ HSCs infiltration and CD68$^+$ Kupffer cells in mouse MASH model.

3.2. STK39 deletion attenuates HFMCD induced liver injury.

To investigate the role of STK39 in MASH, systemic STK39-deficient (STK39$^{-/-}$) mice were established (Figure 2A). These mice were born and developed normally, exhibiting no apparent functional defects (Figure 2B and Figure S1, *http://www.biosciencetrends.com/action/getSupplementalData.php?ID=205*). Subsequently, STK39$^{-/-}$ mice and their control littermates were administered HFMCD diet for 8 weeks. STK39$^{-/-}$ and control mice fed a normal diet served as controls. When fed either a normal diet (ND) or an HFMCD diet, there was a negligible difference in liver morphology and liver-to-body weight ratio between STK39$^{-/-}$ and control mice (Figure 2C and D). Intriguingly, histological examination revealed

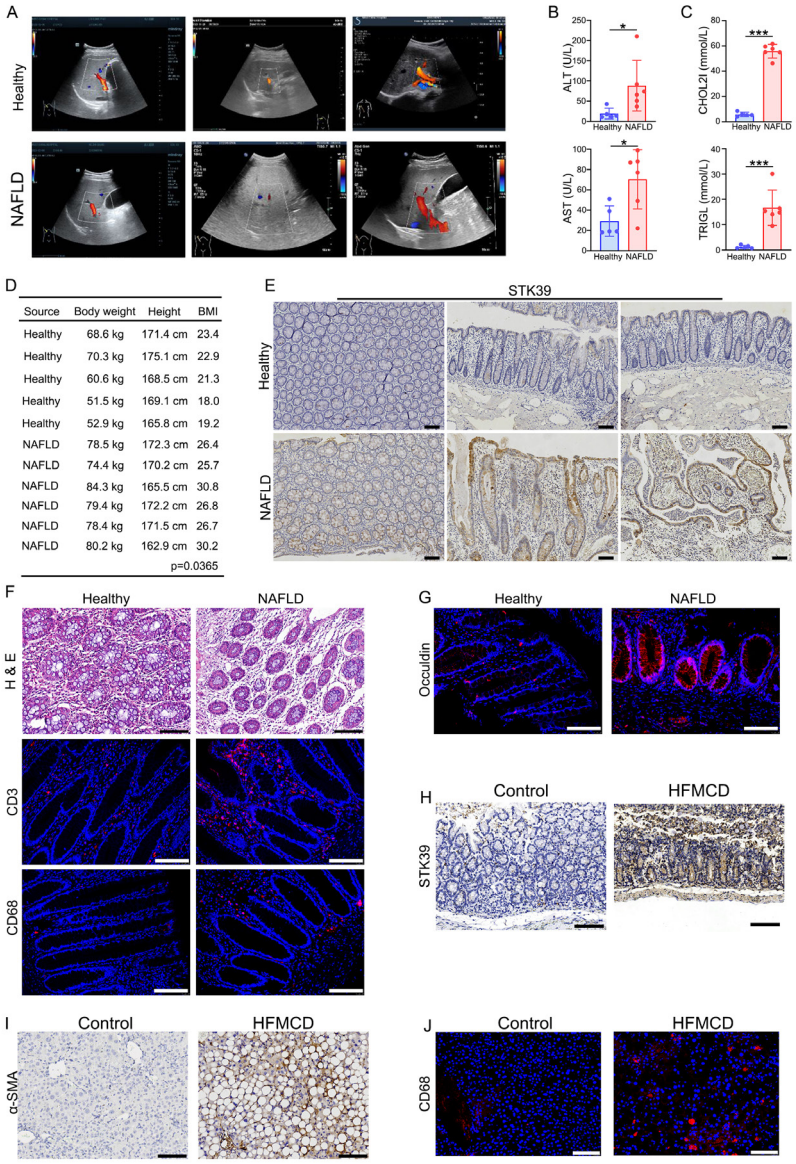

Figure 1. Colonic STK39 expression increased in MASLD patients. (A) Ultrasound imaging of healthy and MASLD patients. **(B)** Serum ALT and AST levels in healthy and MASLD patients. **(C)** Serum CHO2I and TRIGL levels in healthy and MASLD patients. **(D)** The weight, height, and BMI of healthy and MASLD. **(E)** Immunohistochemistry analyses of STK39 in colon tissue sections from healthy and MASLD patients. **(F)** Photomicrographs of H&E-, CD3 and CD68 stained colon tissue sections from healthy and MASLD patients. **(G)** Immunofluorescence analyses of Occuldin in colon tissue sections from healthy and MASLD patients. **(H)** Immunohistochemistry analyses of STK39 in colon tissue sections of ND and 8-week-HFMCD-induced mice. **(I)** Immunofluorescence analyses of α-SMA in liver tissues of ND and 8-week-HFMCD-induced mice. **(J)** Immunohistochemistry analyses of CD68 in liver tissue sections of ND and 8-week-HFMCD-induced mice. Scale bars: 100 μm in (E), (F), (G), (H), (I) and (J). *indicates $p < 0.05$; **indicates $p < 0.01$; ***indicates $p < 0.001$.

that STK39$^{-/-}$ mice developed less severe phenotypes of MASH, as indicated by reduced inflammatory cell infiltration, and decreased incidence of periportal and sinusoidal fibrosis (Figure 2E). Additionally, liver fibrosis marker genes and proteins were also evaluated. As shown in Figure 2F, the expression of α-SMA and TGF-β1 (another profibrogenic protein), was markedly lower in STK39$^{-/-}$ mouse livers. Similarly, the transcript levels of key molecules associated with hepatic fibrogenesis, including tissue inhibitor of metalloproteinase 1 (TIMP-1), and collagen 1 (α1 and α2), were also significantly decreased (Figure 2G). The MASH-CRN scores exhibited a significant decrease of 1.53-fold in STK39$^{-/-}$ mice fed an HFMCD diet compared to control mice fed the same diet (Figure 2H). Furthermore, the serum concentrations of AST and ALT were significantly lower in STK39$^{-/-}$ mice fed an HFMCD diet compared to control mice, with reductions of 2.73-fold and 5.07-fold, respectively (Figure 2I and J).

To unravel the underlying molecular mechanism involved in HFMCD-induced MASH in STK39$^{-/-}$ mice, we employed immunohistochemistry (IHC) to evaluate additional markers of hepatic inflammation. F4/80 and CD68 staining revealed decreased infiltration of hepatic macrophages or Kupffer cells in HFMCD-fed STK39$^{-/-}$ mice (Figure 2K). The results of this study demonstrated

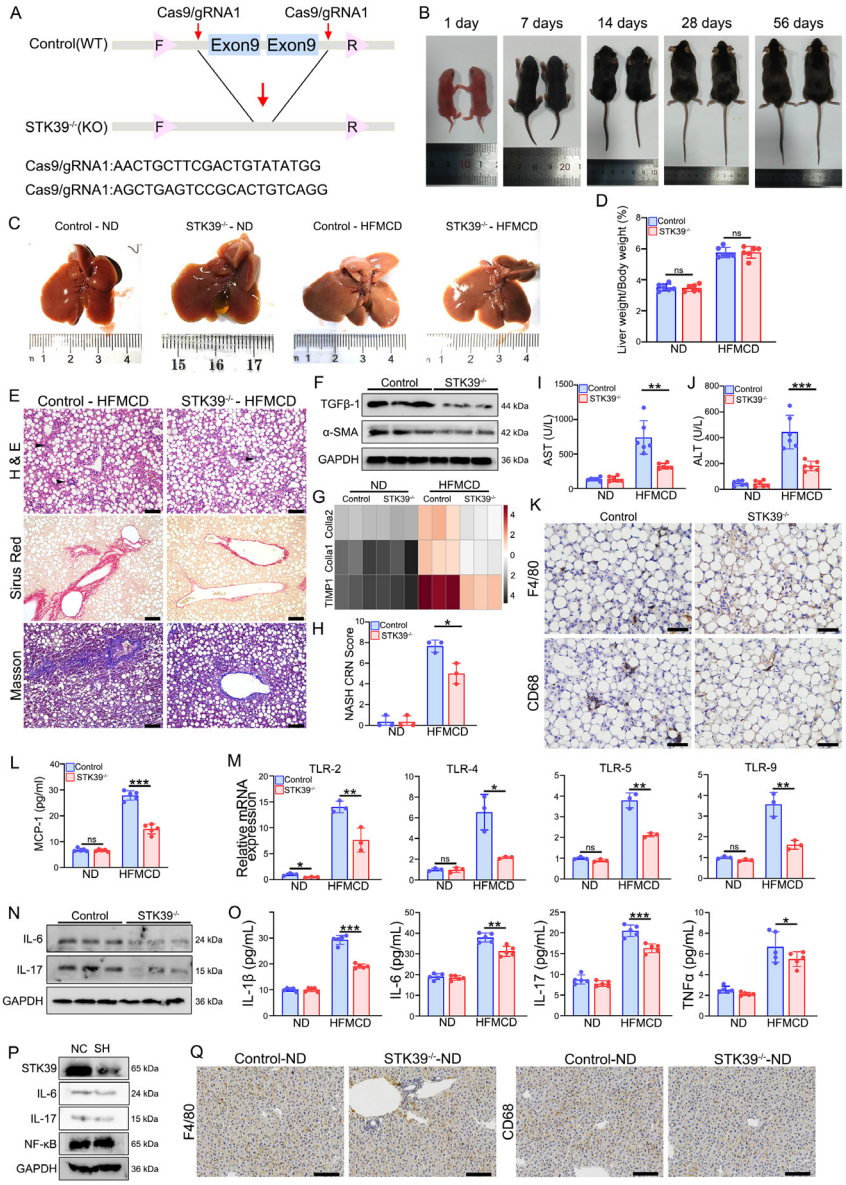

Figure 2. STK39$^{-/-}$ mice fed a HFMCD developed modest histologic features of MASH. (A) Schematic of STK39-knockout in exons 9 and 10 using CRISPR/Cas9. (B) Representative images of control (wild-type [WT]) and STK39$^{-/-}$ mice for 1, 7, 14, 30, and 56 days. **(C)** Representative gross images of livers from WT and STK39$^{-/-}$ mice fed a ND or HFMCD for 8 weeks. **(D)** Liver weight/ Body weight analysis of WT and STK39$^{-/-}$ mice fed a ND or HFMCD for 8 weeks. **(E)** Photomicro-graphs of H&E, Sirus Red, and Masson-stained liver tissue sections of WT and STK39$^{-/-}$ mice fed a HFMCD for 8 weeks (n = 6). **(F)** Western blots demonstrating levels of TGF-β and α-SMA in liver tissues of WT and STK39$^{-/-}$ mice fed a HFMCD for 8 weeks (n = 3). **(G)** Heatmap showing TIMP1, Colla1, and Colla2 mRNA expression in liver tissues of WT and STK39$^{-/-}$ mice fed a ND or HFMCD for 8 weeks (n = 3). **(H)** MASH-CRN score in WT and STK39$^{-/-}$ mice fed a ND or HFMCD for 8 weeks (n = 3). **(I)** Serum AST levels in WT and STK39$^{-/-}$ mice fed a ND or HFMCD for 8 weeks (n = 6). **(J)** Serum ALT levels in the control (wild-type [WT]) and STK39$^{-/-}$ mice fed a ND or HFMCD for 8 weeks (n = 6). **(K)** Immunohistochemical analyses of F4/80 and CD68 in liver tissue sections of WT and STK39$^{-/-}$ mice fed a HFMCD for 8 weeks. **(L)** Quantification of the hepatic monocyte chemoattractant protein 1 (MCP-1) expression in WT and STK39$^{-/-}$ mice fed a normal diet (ND) or a HFMCD for 8 weeks (n = 5). **(M)** QT-PCR showing TLR2, TLR4, TLR5, and TLR9 mRNA expression in liver tissues of WT and STK39$^{-/-}$ mice fed a ND or HFMCD for 8 weeks (n = 3). **(N)** Western blots demonstrating levels of IL-6 and IL-17 in liver tissues of WT and STK39$^{-/-}$ mice fed a HFMCD for 8 weeks (n = 3). **(O)** Serum IL-1β, IL-6, IL-17, and TNFα levels (n = 5). **(P)** Western blots demonstrating the levels of IL-6, IL-17 and NF-κB in PA treated HepG2 cell lines with or without STK39 knockdown. **(Q)** Immunohistochemical analyses of F4/80 and CD68 in liver tissue sections of WT and STK39$^{-/-}$ mice fed a ND. Scale bars: 50 μm in (K) and 100 μm in (E) and (Q). *indicates $p < 0.05$; **indicates $p < 0.01$; ***indicates $p < 0.001$.

a strong association between decreased levels of monocyte chemoattractant protein 1 (MCP-1, 1.87-fold) in the livers of STK39$^{-/-}$ mice fed an HFMCD diet (Figure 2L). Further investigation revealed that the livers of HFMCD-fed STK39$^{-/-}$ mice exhibited significantly reduced expression levels of Toll-like receptors (TLRs)-2 (1.84-fold), TLR-4 (3.02-fold), TLR-5 (1.79-fold), and TLR-9 (2.21-fold), which are the primary TLRs involved in the recognition of bacterial pathogen-associated molecular patterns (Figure 2M). Consistent with these findings, the hepatic protein levels of key proinflammatory cytokines associated with MASH, IL-

6, and IL-17, exhibited a notable decrease in HFMCD-fed STK39$^{-/-}$ mice compared to control mice (Figure 2N). Furthermore, HFMCD-fed STK39$^{-/-}$ mice had significantly lower circulating levels of IL-1β (1.53-fold), IL-6 (1.21-fold), IL-17 (1.26-fold), and tumor necrosis factor-α (TNFα, 1.21-fold) (Figure 2O).

Conversely, in palmitic acid (PA)-treated HepG2 cells, there was no discernible difference in the levels of proinflammatory cytokines (IL-6 and IL-17) and transcription factor (NF-κB) between cells with or without STK39 expression (Figure 2P). Taken together, these findings suggest that TLR-mediated activation and recruitment of innate immune system cells are the causes of decreased hepatic inflammation in HFMCD-fed STK39$^{-/-}$ mice. However, no differences in hepatic inflammatory parameters or immune cell infiltration were observed between control and STK39$^{-/-}$ mice fed a normal diet (Figure 2Q).

Interestingly, for both the ND and HFMCD diet-fed mice, no difference was found in lipid droplet accumulation in the liver of both genotypes of mice (Figure 3A). Liver histopathology (Figure 3B), serum biochemical parameters of MASH, and molecular markers of fibrosis did not significantly differ between normal diet-fed control and STK39$^{-/-}$ mice (Figure 2G-J). No significant differences were observed with respect to metabolic parameters, including cholesterol (CHO2I) or triglyceride (TRIGL) levels (Figure 3C and D). In addition, the expression of genes involved in de novo lipogenesis (Fas and Pparα), lipid transport (Cpt1a), and β-oxidation (Acox1) were also not significantly lower in STK39$^{-/-}$ mice than in HFMCD-fed controls (Figure 3E). Furthermore, we evaluated the impact of STK39 knockdown on lipid metabolism *in vitro*. In a palmitic acid (PA)-induced MASH model, STK39 knockdown *via* short-hairpin RNA (shRNA) had little impact on lipid accumulation in HepG2 cells (Figure 3F).

In summary, STK39 Knockout mice reduced HFMCD-induced liver inflammation but had minimal effects on hepatic lipid metabolism.

3.3. STK39 ablation improves intestinal epithelial permeability in HFMCD mouse model.

HFMCD consumption causes damage to the intestinal epithelial barrier, leading to increased translocation of gut-associated microbial products and consequent excessive hepatic inflammation. The attenuated hepatic inflammation in STK39$^{-/-}$ mice prompted us to determine whether STK39 impairs the intestinal epithelial barrier. We measured intestinal epithelial permeability using an *in vivo* FITC-dextran permeability assay, and the serum lipopolysaccharide (LPS) concentration was used as an indicator of increased microbial product translocation. Compared with that in normal diet-fed WT mice, the dextran flux in HFMCD-

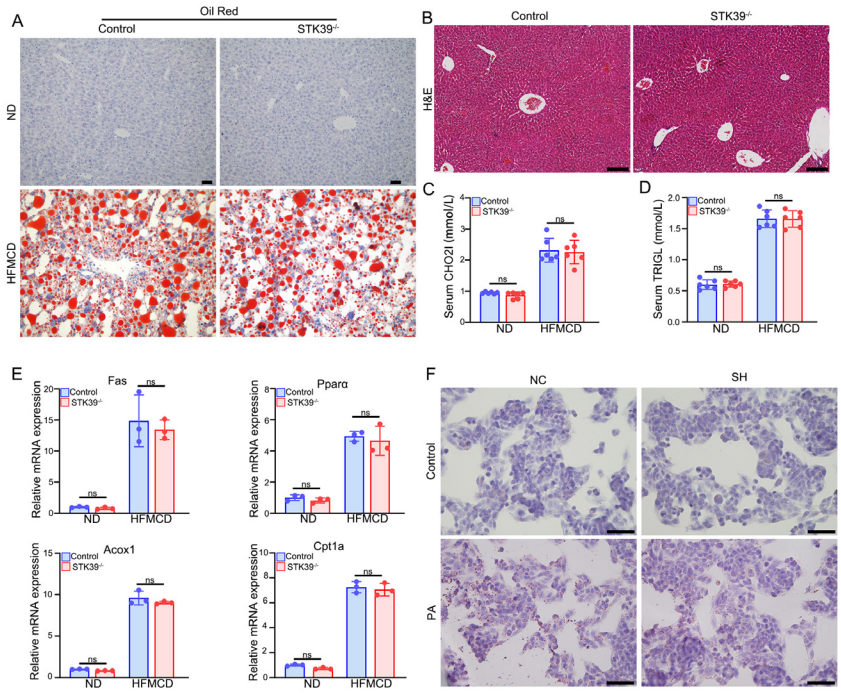

Figure 3. STK39$^{-/-}$ mice exhibited no significant differences in lipid metabolism. (A) Photomicrographs of Oil Red-stained liver tissue sections of WT and STK39$^{-/-}$ mice fed a ND or HFMCD for 8 weeks. **(B)** Photomicrographs of H&E-stained liver tissue sections of WT and STK39$^{-/-}$ mice fed a ND. **(C)** Serum CHO2I levels of WT and STK39$^{-/-}$ mice fed a ND or HFMCD for 8 weeks. **(D)** Serum TRIGL levels of WT and STK39$^{-/-}$ mice fed a ND or HFMCD for 8 weeks. **(E)** Quantification of the Fas, Pparα, Acox1, and Cpt1a expression in WT and STK39$^{-/-}$ mice fed a normal diet (ND) or a HFMCD for 8 weeks. **(F)** Photomicrographs of Oil Red-stained HepG2 cell lines of PA treated with or without STK39 knockout. Scale bars: 50 μm in (F) and 100 μm in (A) and (B). *indicates $p < 0.05$; **indicates $p < 0.01$; ***indicates $p < 0.001$.

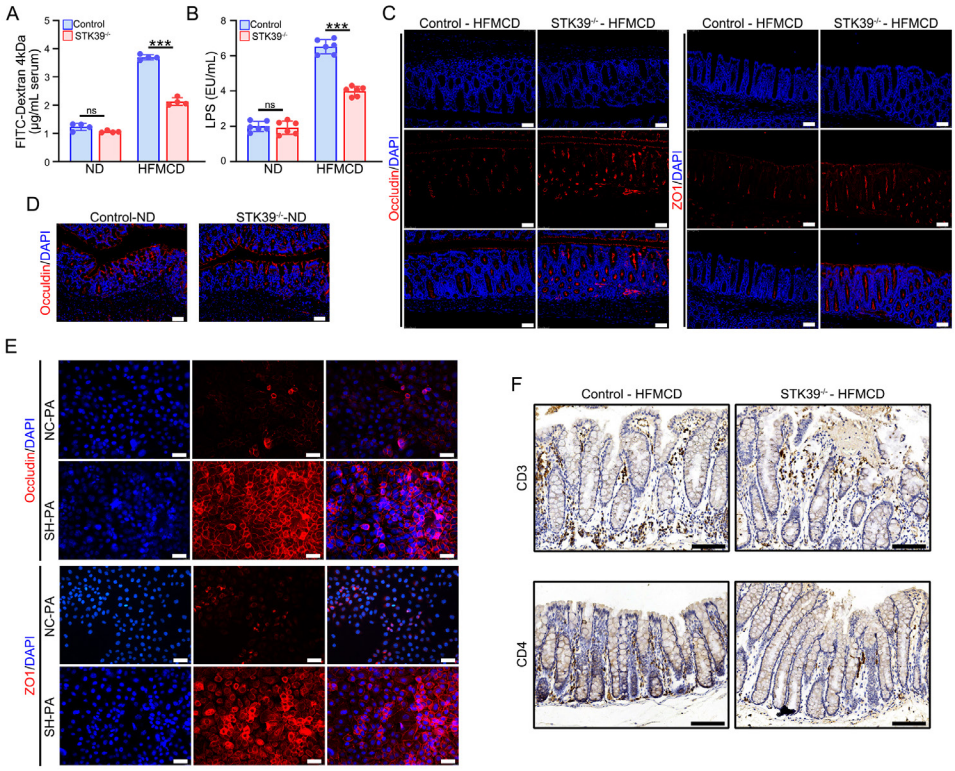

Figure 4. STK39-ablation attenuated HFMCD-induced intestinal epithelial permeability and bacterial translocation. (A) Intestinal permeability to FITC-dextran in WT and STK39$^{-/-}$ mice fed a normal diet (ND) or a HFCD for 8 weeks (n = 4). **(B)** Serum LPS levels after 8 weeks of ND and HFMCD feeding (n = 6). **(C)** Immunofluorescence analyses of Occludin and ZO1 in colon tissue sections of WT and STK39$^{-/-}$ mice fed a HFMCD for 8 weeks. **(D)** Immunofluorescence analyses of Occludin in colon tissue sections of WT and STK39$^{-/-}$ mice fed a ND for 8 weeks. **(E)** Immunofluo-rescence analyses of Occludin and ZO1 in SW480 cell lines of control and STK39 knockdown treated with PA. **(F)** Immunohistochemistry analyses of CD3 and CD4 in colon tissue sections of WT and STK39$^{-/-}$ mice fed a HFMCD for 8 weeks. Scale bars: 50 μm in (C), (D), (E), and (F). *indicates $p < 0.05$; **indicates $p < 0.01$; ***indicates $p < 0.001$.

fed WT mice was 3-fold greater, but the dextran flux in HFMCD-fed STK39$^{-/-}$ mice was much lower (1-fold) (Figure 4A). This indicated that consumption of HFMCD led to impairment of intestinal epithelial barrier function, and knockout of STK39 alleviated this injury, thereby delaying MASH development in STK39$^{-/-}$ mice. Similarly, we also observed a 1.63-fold reduction in the serum LPS concentration in HFMCD-fed STK39$^{-/-}$ mice compared to that in HFMCD-fed control mice (Figure 4B).

Additionally, the expression and distribution of the tight junction proteins (Occludin and ZO-1) were determined *via* immunofluorescence. As shown in Figure 4C, Occludin and ZO-1 expression was more intact in HFMCD-fed STK39$^{-/-}$ mice, compared with HFMCD-fed control mice. However, no significant difference in Occludin expression was observed between the two genotypic mouse strains fed a normal diet (Figure 4D). To further explore the role of STK39 in regulating tight junctions (TJs), STK39 was silenced in SW480 cells, a colorectal cancer cell line. Consistent with the findings *in vivo*, STK39 knockdown led to maintained Occludin and ZO-1 expression in PA-treated model (Figure 4E). In addition to protecting TJs, knockout of STK39 in mice also suppressed HFMCD-induced intestinal inflammation (Figure 4F).

Taken together, these findings suggest that STK39 plays a negative role in intestinal barrier integrity.

3.4. STK39 knockout delays MASH formation in the HFD+DSS-induced model.

As shown above, HFMCD can impair the intestinal barrier, which promotes MASH development. Colitis is primarily characterized by damage to the intestinal barrier and is caused by the administration of dextran sulfate sodium (DSS) in mice (*23*). A high-fat diet (HFD) is commonly used to induce MASLD without liver fibrosis and less inflammatory cell infiltration compared with HFMCD. To further investigate the association between intestinal barrier integrity and MASH, STK39$^{-/-}$ and control mice were fed a HFD or HFD + DSS (1%) for 4 weeks (Figure 5A). Compared with those in the HFD group, the mice in the HFD + DSS group developed more severe histological features of MASH, including liver fibrosis and inflammatory cell infiltration, suggesting that the combination of HFD and DSS could trigger MASH (Figure 5B-D). Notably, ablation of STK39 significantly reduced MASH incidence, as indicated by fibrosis and inflammatory cell infiltration (Figure 5E and F), even

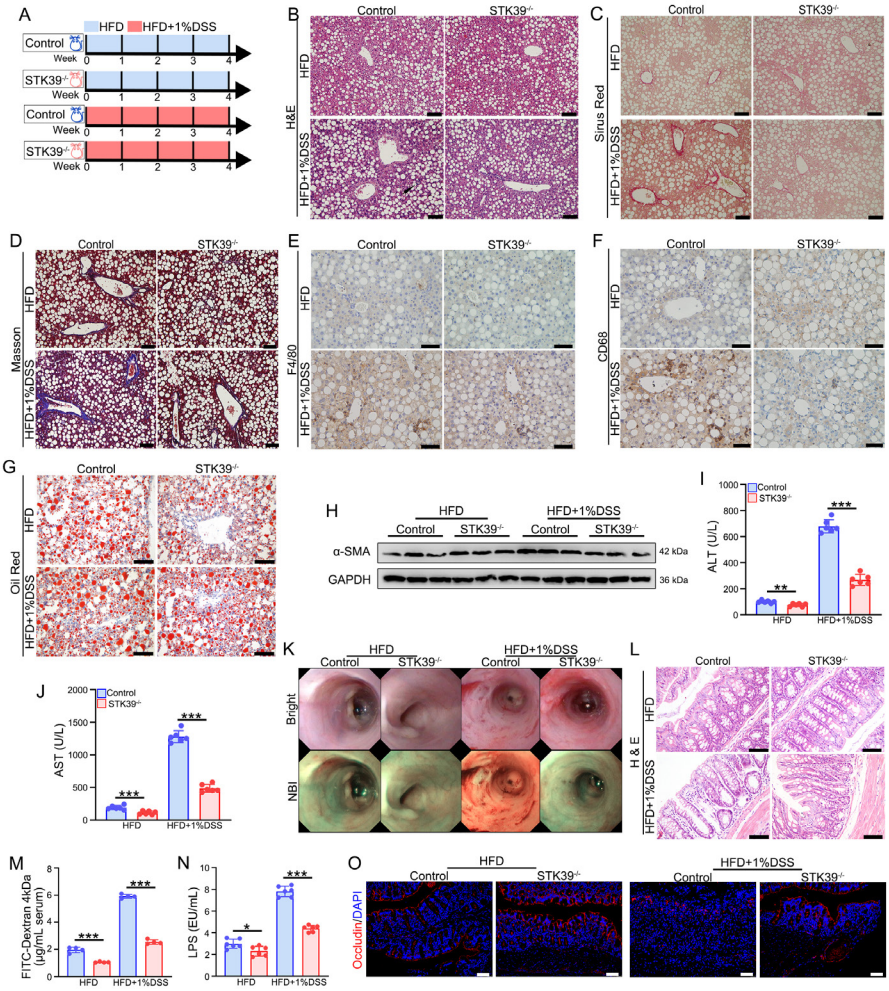

Figure 5. STK39 knockout delayed MASH in the HFD+DSS-induced model. (A) Schematic of the WT and STK39$^{-/-}$ mice and experiment protocol; DSS: 1%. **(B)** Photomicrographs of H&E-stained liver tissue sections of WT and STK39$^{-/-}$ mice fed a HFD and HFD+DSS for 4 weeks (n = 6). **(C)** Photomicrographs of Sirus Red-stained liver tissue sections of WT and STK39$^{-/-}$ mice fed a HFD and HFD+DSS for 4 weeks. **(D)** Photomicrographs of Masson-stained liver tissue sections of WT and STK39$^{-/-}$ mice fed a HFD and HFD+DSS for 4 weeks. **(E)** Immunohistochemistry analyses of F4/80 in liver tissue sections of WT and STK39$^{-/-}$ mice fed a HFD and HFD+DSS for 4 weeks. **(F)** Immunohistochemistry analyses of CD68 in liver tissue sections of WT and STK39$^{-/-}$ mice fed a HFD and HFD+DSS for 4 weeks. **(G)** Photomicrographs of Oil Red-stained liver tissue sections of WT and STK39$^{-/-}$ mice fed a HFD or HFD+DSS for 4 weeks. **(H)** Western blots demonstrating lev-els of α-SMA in liver tissues of WT and STK39$^{-/-}$ mice fed a HFD and HFD+DSS for 4 weeks. **(I, J)** Serum ALT AND AST levels in the WT and STK39$^{-/-}$ mice fed a HFD and HFD+DSS for 4 weeks (n = 6). **(K)** Representative morphology images of colonoscopy from WT and STK39$^{-/-}$ mice fed a HFD or HFD+DSS for 4 weeks. **(L)** Photomicrographs of H&E-stained colon tissue sections of WT and STK39$^{-/-}$ mice fed a HFD or HFD+DSS for 4 weeks. **(M)** Intestinal permeability to FITC-dextran in WT and STK39$^{-/-}$ mice fed a HFD or HFD+DSS for 4 weeks. **(N)** Serum LPS levels in WT and STK39$^{-/-}$ mice fed a HFD or HFD+DSS for 4 weeks. **(O)** Immunofluorescence analyses of Occludin in WT and STK39$^{-/-}$ mice fed a HFD or HFD+DSS for 4 weeks. Scale bars: 50 μm in (E), (F), (G), (L), and (O); 100 μm in (B), (C), and (D). *indicates $p < 0.05$; **indicates $p < 0.01$; ***indi-cates $p < 0.001$.

though the accumulation of lipids was unaffected (Figure 5G). Consistent with the findings in HFMCD-induced MASH, the α-SMA protein expression showed that ablation of STK39 significantly reduced fibrosis (Figure 5H). Furthermore, the serum AST and ALT concentrations were also significantly lower in STK39$^{-/-}$ mice than in WT mice (Figure 5I and J).

Moreover, colonoscopy and histological analysis revealed milder colonic damage in STK39$^{-/-}$ mice (Figure 5K and L). The dextran flux and serum LPS levels were lower in STK39$^{-/-}$ mice than in control mice, regardless of DSS administration (Figure 5M and N). Additionally, the expression of Occludin was much greater in STK39$^{-/-}$ mice in both the HFD and HFD + DSS (1%) groups (Figure 5O). Taken together, these data provide evidence that STK39 ablation can alleviate MASH induced by HFD and DSS by reducing intestinal barrier disruption caused by DSS.

3.5. ZT-1a attenuates HFMCD induced liver injury by improving intestinal epithelia permeability.

The above results prompted us to investigate whether inhibiting STK39 activity prevents the progression of MASH. Mice were treated with 100 mg/kg ZT-1a, a specific STK39 inhibitor, through intraperitoneal

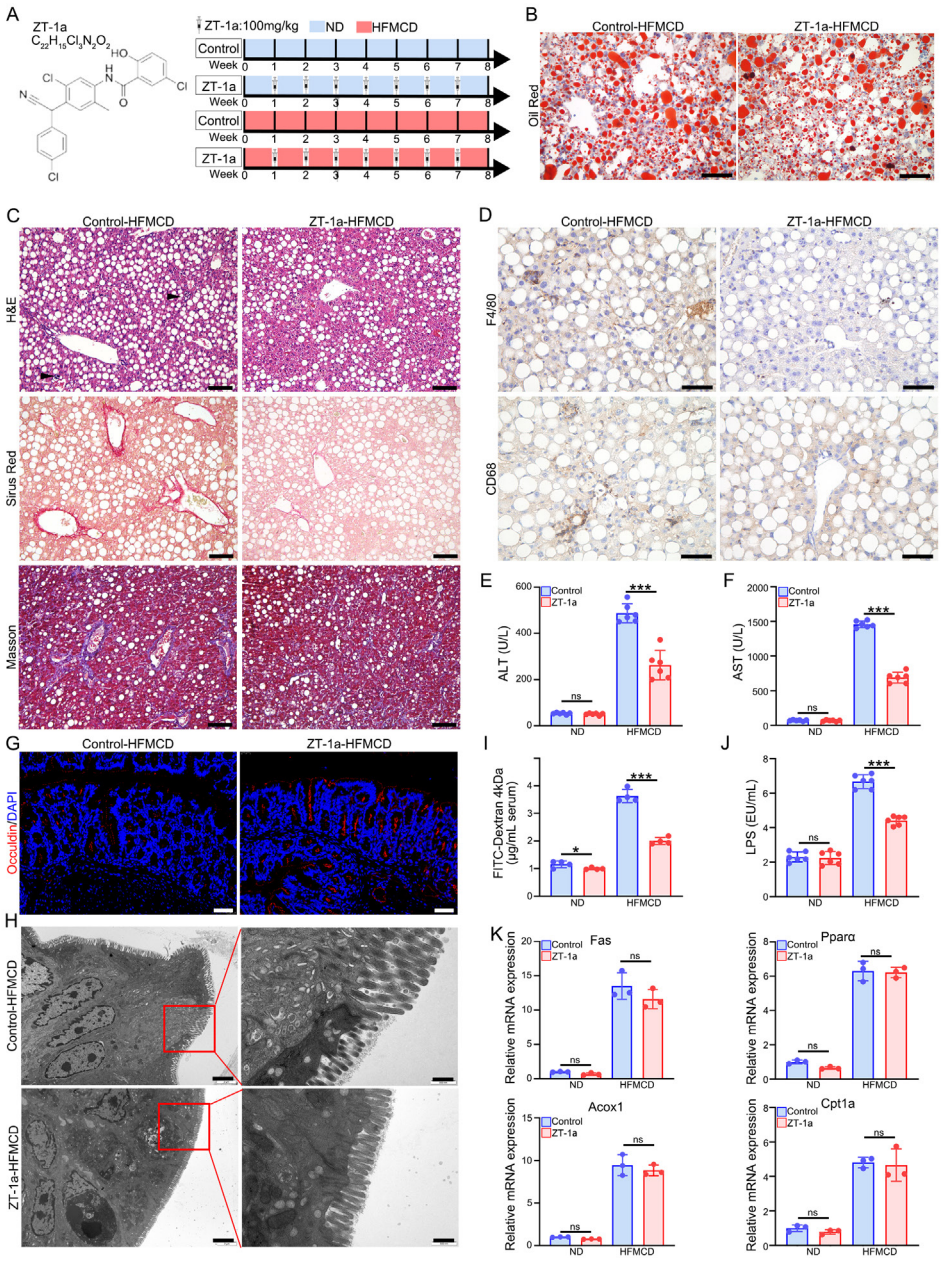

Figure 6. STK39 inhibition by ZT-1a attenuated HFMCD-induced MASH. (A) Structural formula of ZT-1a and schematic of the experiment protocol. **(B)** Oil Red O staining of steatosis in liv-er tissues of control and ZT-1a treated mice fed a HFMCD for 8 weeks. **(C)** Photomicrographs of H&E, Sirus Red O and Masson-stained liver tissue sections of control and ZT-1a treated mice fed a HFMCD for 8 weeks. (n = 6). **(D)** Immunohistochemistry analyses of F4/80 and CD68 in liver tissue sections of control and ZT-1a treated mice fed a HFMCD for 8 weeks. **(E, F)** Serum ALT and AST levels in the control and ZT-1a treated mice fed a HFMCD for 8 weeks (n = 6). Scheme of the Con-trol and STK39$^{-/-}$ mice and experiment protocol; DSS:1%. **(G)** Immunofluorescence analyses of Occludin in liver tissue sections of control and ZT-1a treated mice fed a HFMCD for 8 weeks. **(H)** Transmission electron microscopy analyses of TJs in colon tissue sections of control and ZT-1a treated mice fed a HFMCD for 8 weeks. **(I)** Intestinal permeability to FITC-dextran in the control and ZT-1a treated mice fed a HFMCD for 8 weeks (n = 4). **(J)** Serum LPS levels in the control and ZT-1a treated mice fed a HFMCD for 8 weeks (n = 6). **(K)** Quantification of the Fas, Pparα, Acox1, and Cpt1a expression in Control and ZT-1a treated mice fed a HFMCD for 8 weeks. Scale bars: 50 μm in (B), (D) and (G); 100 μm in (C); 2 μm (left) and 500 nm (right) in (H). Statistics: Unpaired two-tailed Student's t test in (E), (F), (H), and (I). *indicates $p < 0.05$; **indicates $p < 0.01$; ***indicates $p < 0.001$.

injection after 1 week of HFMCD treatment (*24*) (Figure 6A). Although no significant differences were observed in steatosis between the control group and the ZT-1a treatment group (Figure 6B), liver fibrosis and inflammation were significantly reduced after ZT-1a treatment, as assessed by H&E, Masson, Sirius Red, F4/80, and CD68 staining (Figure 6C and D). Consistent with these results, the serum ALT and AST levels were also lower in ZT-1a-treated mice than in control mice (Figure 6E and F). As expected, ZT-1a protected TJs against HFMCD-induced impairment, as measured by Occludin immunofluorescence staining (Figure 6G). We further examined the TJs by transmission electron microscopy. Consistently, we

found ZT-1a protected the TJs (Figure 6H). Similarly, the serum dextran flux and LPS concentration in the ZT-1A-treated mice were 1.74-fold and 1.51-fold lower, respectively, than those in the control group (Figure 6I and J). Interestingly, ZT-1a also had minimal impact in the lipid metabolism pathway (Figure 6K).

4. Discussion

In the present study, we present experimental evidence indicating that intestinal epithelial barrier function plays a pivotal role in the progression of MASLD. STK39 was overexpressed in colon tissues from MASH patients and mice. Knockout of STK39 and inhibition of STK39 activity using ZT-1a significantly alleviated HFMCD-induced MASH in mice by reducing hepatic inflammation and fibrosis. Mechanistically, the knockout of STK39 ameliorated MASH through the attenuation of gut inflammation, enhancement of intestinal barrier functions and decreased intestinal bacterial translocation (Figure 7).

The incidence of MASH, which increases the risk of diabetes, cardiovascular diseases, and cancer, is rising worldwide (*25*). Consequently, it is imperative to explore therapeutic targets aimed at preventing adverse outcomes. STK39 is a serine/threonine kinase believed to function within the cellular stress response pathway. The kinase becomes activated in response to hypotonic stress, triggering the phosphorylation of several cation-chloride-coupled cotransporters. The catalytically active form of STK39 specifically activates the p38 MAP kinase pathway, and its interaction with p38 diminishes during cellular stress, indicating that this kinase may serve as a mediator in the cellular stress response (*26,27*). In our research, when STK39 was systemically knocked out, the progression of hepatic fibrosis and inflammation caused by the HFMCD diet was markedly inhibited. This inhibition was similar to the phenotype observed following intestinal knockout of STK39. MASH is generally considered to be the outcome of excessive accumulation of hepatic lipids, leading to hepatocyte rupture and death, as well as the recruitment of inflammatory factors that exacerbate the development of hepatic inflammation and fibrosis (*28*). However, we discovered that hepatic genes pertaining to lipid metabolism, encompassing those involved in de novo lipogenesis, transport, and β-oxidation, were not significantly altered when STK39 was knocked out either *in vivo* or *in vitro*. This suggested that STK39 does not affect lipid metabolism in the liver. We subsequently delved deeper into the changes in the expression of STK39 in the liver during the development of MASH. Our findings revealed that STK39 expression was not significantly upregulated when hepatic inflammation was not evident. Nevertheless, the protein level of STK39 was significantly elevated in the presence of increased macrophage infiltration (Figure S2, *http://www.biosciencetrends.com/action/getSupplementalData.php?ID=205*). This may be attributed to the fact that when hepatic inflammation becomes apparent, proinflammatory factors such as NF-κB upregulate the expression of STK39, which subsequently exacerbates the progression of hepatic inflammation and fibrosis, which aligns with previous reports by Tsai-Jung Lin (*29*). Collectively, our findings confirm that STK39 is not involved in the progression of MASH through its influence on lipid metabolism. Consequently, these findings prompted us to explore novel mechanisms underlying how STK39 contributes to the progression of MASH.

Bidirectional crosstalk along the gut-liver axis controls gastrointestinal health and disease, exploiting environmental and host mediators (*7*). Nutrients,

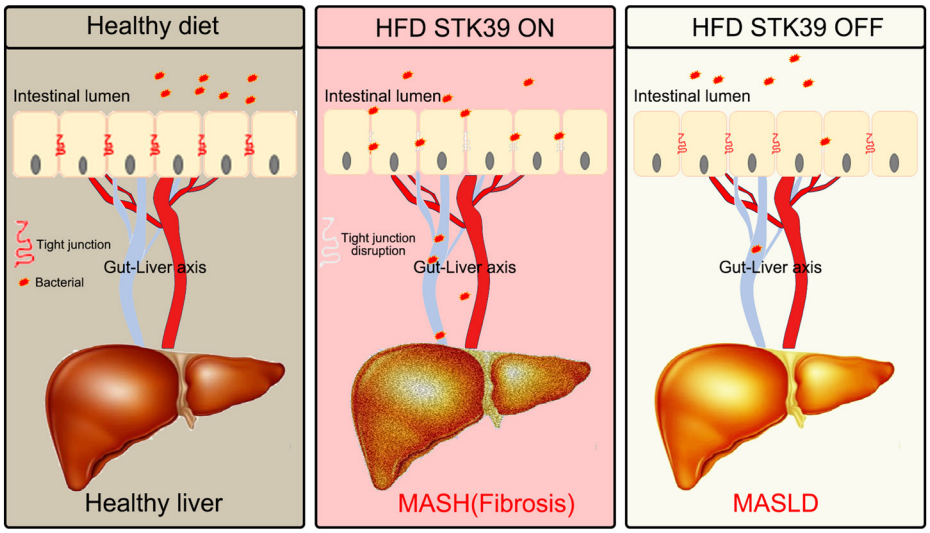

Figure 7. Modulation of intestinal epithelial permeability by STK39 promotes MAFLD /MASH progression.

microbial antigens, metabolites, and bile acids modulate metabolism and immune responses in both the gut and liver, which in turn mutually influence the structure and function of the microbial community. Perturbation in these host-microbe interactions are observed in various experimental liver diseases and are exacerbated by an impaired intestinal barrier, which fuels hepatic inflammation and disease progression (*30*). Clinical evidence demonstrates perturbation of the gut-liver crosstalk in MASLD, alcoholic liver disease, and primary sclerosing cholangitis (*31*). In liver cirrhosis, a common sequela of these diseases, the intestinal microbiota and microbial pathogen-associated molecular patterns contribute to liver inflammation and clinical complications (*32*). Recent studies have shown that STK39 expression is enhanced in colon tissues from patients with Crohn's disease (CD) and ulcerative colitis (UC) (*21*). Notably, the intestinal barrier is significantly impaired in CD and UC patients. Numerous studies have reported that intestinal barrier damage is linked to liver disease, including MASLD/MASH, liver cirrhosis, and hepatocellular carcinoma (*33-35*). We discovered that suppressing STK39 protected the intestinal barrier and reduced inflammatory cell infiltration in colonic tissues. Thess findings suggest that STK39 may be involved in the development of MASH through intestinal barrier damage. Moreover, STK39 knockout protected tight junction proteins (Occludin and ZO1) from HFD-induced damage. These findings indicate that STK39 may negatively regulate the intestinal barrier integrity. The HFD+DSS model further supports our hypothesis. A HFD reduces tight junction proteins in the gut, but only causes mild inflammation and fibrosis in the liver. We found that the combination of HFD+DSS led to significant MASH symptoms, including severe inflammation and fibrosis. Moreover, the clearance of STK39 significantly inhibited the damage to intestinal tight junction proteins caused by HFD+DSS. The serum LPS concentration was reduced, and intestinal bacterial translocation was also significantly reduced. Eventually, the degree of liver fibrosis and inflammation are significantly attenuated, strongly delaying the progression of MASH. Although we have demonstrated that STK39 is associated with tight junction proteins, the exact mechanism by which STK39 regulates the expression of these proteins needs to be further explored. Given the crucial role of STK39 in the gut-liver axis, it may represent a novel target for the treatment of MASH.

There is also growing evidence that drugs developed to target the intestinal barrier, such as those for MASLD/MASH, can be effective in treating liver disease (*36*). Here, we chose the pharmacological inhibitor, ZT-1a, a potent non-ATP-competitive and selective SPAK inhibitor that inhibits STK39 activity, which has been shown to effectively and efficiently improve neurological function after ischemic stroke (*24*). In the present study, we found that after ZT-1a treatment, the level of tight junction proteins in the intestinal epithelium was maintained, and the intestinal barrier was protected, thereby reducing hepatic fibrosis and inflammatory cell infiltration and effectively slowing the progression of MASH. These findings not only strongly demonstrate the important role of STK39 in MASH, but also provide a new therapeutic strategy for treating MASH.

Taken together, our work demonstrates a crucial role for intestinal epithelial permeability in MASH progression and underscores the intricate role of diet in regulating gut homeostasis, inflammation, and liver health. Given our data showing increased STK39 expression in colonic biopsy specimens from MASLD patients, it suggests that genetic or epigenetic vulnerabilities of proteins regulating intestinal epithelial barrier integrity may predispose human to MASLD progression. In conclusion, our data have revealed that defective intestinal epithelial barrier, dysbiosis, and associated activation of the innate immune system caused by increased translocation of gut microbial products are risk factors associated with MASLD progression. Mice fed HFMCD diet exhibited a superimposed hit, driving a proinflammatory gut microbial composition that exacerbated gut permeability. In turn, enhanced gut leakiness results in microbial product translocation, which induces hepatic inflammation and injury, ultimately leading to the progression of MASLD to MASH. STK39 inhibition prevented this process. The present findings strongly justify the consideration of therapies targeting the intestinal epithelial barrier, dysbiosis, innate immune function, or a combination of these factor to significantly slow or halt MASH progression.

Funding: This work was supported by a grant from the Science Foundation of Sichuan, China (NO.2023NSFSC1613) and the Postdoctoral Foundation of West China Hospital, Sichuan University (NO. 2023HXBH020).

Conflict of Interest: The authors have no conflicts of interest to disclose.

References

1. Ray K. NAFLD-the next global epidemic. Nat Rev Gastroenterol Hepatol. 2013; 10:621.
2. Younossi Z, Tacke F, Arrese M, Chander Sharma B, Mostafa I, Bugianesi E, Wai-Sun Wong V, Yilmaz Y, George J, Fan J, Vos MB. Global Perspectives on Nonalcoholic Fatty Liver Disease and Nonalcoholic Steatohepatitis. Hepatology. 2019; 69:2672-2682.
3. Anstee QM, Reeves HL, Kotsiliti E, Govaere O, Heikenwalder M. From NASH to HCC: current concepts and future challenges. Nat Rev Gastroenterol Hepatol. 2019; 16:411-428.

4. De Munck TJI, Xu P, Verwijs HJA, Masclee AAM, Jonkers D, Verbeek J, Koek GH. Intestinal permeability in human nonalcoholic fatty liver disease: A systematic review and meta-analysis. Liver Int. 2020; 40:2906-2916.
5. Rahman K, Desai C, Iyer SS, Thorn NE, Kumar P, Liu Y, Smith T, Neish AS, Li H, Tan S, Wu P, Liu X, Yu Y, Farris AB, Nusrat A, Parkos CA, Anania FA. Loss of Junctional Adhesion Molecule A Promotes Severe Steatohepatitis in Mice on a Diet High in Saturated Fat, Fructose, and Cholesterol. Gastroenterology. 2016; 151:733-746.e12.
6. He S, Cui S, Song W, Jiang Y, Chen H, Liao D, Lu X, Li J, Chen X, Peng L. Interleukin-17 Weakens the NAFLD/NASH Process by Facilitating Intestinal Barrier Restoration Depending on the Gut Microbiota. mBio. 2022; 13:e0368821.
7. Albillos A, de Gottardi A, Rescigno M. The gut-liver axis in liver disease: Pathophysiological basis for therapy. J Hepatol. 2020; 72:558-577.
8. Leshem A, Liwinski T, Elinav E. Immune-Microbiota Interplay and Colonization Resistance in Infection. Mol Cell. 2020; 78:597-613.
9. Moreira AP, Texeira TF, Ferreira AB, Peluzio Mdo C, Alfenas Rde C. Influence of a high-fat diet on gut microbiota, intestinal permeability and metabolic endotoxaemia. Br J Nutr. 2012; 108:801-809.
10. Pendyala S, Walker JM, Holt PR. A high-fat diet is associated with endotoxemia that originates from the gut. Gastroenterology. 2012; 142:1100-1101.e2.
11. Otani T, Furuse M. Tight Junction Structure and Function Revisited. Trends Cell Biol. 2020; 30:805-817.
12. Buckley A, Turner JR. Cell Biology of Tight Junction Barrier Regulation and Mucosal Disease. Cold Spring Harb Perspect Biol. 2018; 10:a029314.
13. Kaushal K, Agarwal S, Sharma S, Goswami P, Singh N, Sachdev V, Poudel S, Das P, Yadav R, Kumar D, Pandey G, Gunjan D, Saraya A. Demonstration of Gut-Barrier Dysfunction in Early Stages of Non-alcoholic Fatty Liver Disease: A Proof-Of-Concept Study. J Clin Exp Hepatol. 2022; 12:1102-1113.
14. Luther J, Garber JJ, Khalili H, Dave M, Bale SS, Jindal R, Motola DL, Luther S, Bohr S, Jeoung SW, Deshpande V, Singh G, Turner JR, Yarmush ML, Chung RT, Patel SJ. Hepatic Injury in Nonalcoholic Steatohepatitis Contributes to Altered Intestinal Permeability. Cell Mol Gastroenterol Hepatol. 2015; 1:222-232.
15. Csak T, Ganz M, Pespisa J, Kodys K, Dolganiuc A, Szabo G. Fatty acid and endotoxin activate inflammasomes in mouse hepatocytes that release danger signals to stimulate immune cells. Hepatology. 2011; 54:133-144.
16. Henao-Mejia J, Elinav E, Jin C, Hao L, Mehal WZ, Strowig T, Thaiss CA, Kau AL, Eisenbarth SC, Jurczak MJ, Camporez JP, Shulman GI, Gordon JI, Hoffman HM, Flavell RA. Inflammasome-mediated dysbiosis regulates progression of NAFLD and obesity. Nature. 2012; 482:179-185.
17. Tsukita S, Furuse M, Itoh M. Multifunctional strands in tight junctions. Nat Rev Mol Cell Biol. 2001; 2:285-293.
18. Pitman RS, Blumberg RS. First line of defense: the role of the intestinal epithelium as an active component of the mucosal immune system. J Gastroenterol. 2000; 35:805-814.
19. Wang W, Zhao J, Gui W, Sun D, Dai H, Xiao L, Chu H, Du F, Zhu Q, Schnabl B, Huang K, Yang L, Hou X. Tauroursodeoxycholic acid inhibits intestinal inflammation and barrier disruption in mice with non-alcoholic fatty liver disease. Br J Pharmacol. 2018; 175:469-484.
20. Johnston AM, Naselli G, Gonez LJ, Martin RM, Harrison LC, DeAizpurua HJ. SPAK, a STE20/SPS1-related kinase that activates the p38 pathway. Oncogene. 2000; 19:4290-4297.
21. Zhang Y, Viennois E, Xiao B, Baker MT, Yang S, Okoro I, Yan Y. Knockout of Ste20-like proline/alanine-rich kinase (SPAK) attenuates intestinal inflammation in mice. Am J Pathol. 2013; 182:1617-1628.
22. Yan Y, Laroui H, Ingersoll SA, Ayyadurai S, Charania M, Yang S, Dalmasso G, Obertone TS, Nguyen H, Sitaraman SV, Merlin D. Overexpression of Ste20-related proline/alanine-rich kinase exacerbates experimental colitis in mice. J Immunol. 2011; 187:14961-505.
23. Zhang J, Bhuiyan MIH, Zhang T *et al*. Modulation of brain cation-Cl− cotransport *via* the SPAK kinase inhibitor ZT-1a. Nature Communications. 2020; 11:78.
24. Bhuiyan MIH, Fischer S, Patel SM, Oft H, Zhang T, Foley LM, Zhang J, Hitchens TK, Molyneaux BJ, Deng X, Sun D. Efficacy of novel SPAK inhibitor ZT-1a derivatives (1c, 1d, 1g & 1h) on improving post-stroke neurological outcome and brain lesion in mice. Neurochem Int. 2023; 162:105441.
25. Harrison SA, Allen AM, Dubourg J, Noureddin M, Alkhouri N. Challenges and opportunities in NASH drug development. Nat Med. 2023; 29:562-573.
26. Rinehart J, Maksimova YD, Tanis JE, Stone KL, Hodson CA, Zhang J, Risinger M, Pan W, Wu D, Colangelo CM, Forbush B, Joiner CH, Gulcicek EE, Gallagher PG, Lifton RP. Sites of regulated phosphorylation that control K-Cl cotransporter activity. Cell. 2009; 138:525-536.
27. Richardson C, Rafiqi FH, Karlsson HK, Moleleki N, Vandewalle A, Campbell DG, Morrice NA, Alessi DR. Activation of the thiazide-sensitive Na+-Cl- cotransporter by the WNK-regulated kinases SPAK and OSR1. J Cell Sci. 2008; 121(Pt 5):675-684.
28. Xu X, Poulsen KL, Wu L, Liu S, Miyata T, Song Q, Wei Q, Zhao C, Lin C, Yang J. Targeted therapeutics and novel signaling pathways in non-alcohol-associated fatty liver/steatohepatitis (NAFL/NASH). Signal Transduct Target Ther. 2022; 7:287.
29. Lin TJ, Yang SS, Hua KF, Tsai YL, Lin SH, Ka SM. SPAK plays a pathogenic role in IgA nephropathy through the activation of NF-κB/MAPKs signaling pathway. Free Radic Biol Med. 2016; 99:214-224.
30. de Vos WM, Tilg H, Van Hul M, Cani PD. Gut microbiome and health: mechanistic insights. Gut. 2022; 71:1020-1032.
31. Tilg H, Adolph TE, Trauner M. Gut-liver axis: Pathophysiological concepts and clinical implications. Cell Metab. 2022; 34:1700-1718.
32. Tilg H, Zmora N, Adolph TE, Elinav E. The intestinal microbiota fuelling metabolic inflammation. Nat Rev Immunol. 2020; 20:40-54.
33. Tilg H, Adolph TE, Dudek M, Knolle P. Non-alcoholic fatty liver disease: the interplay between metabolism, microbes and immunity. Nat Metab. 2021; 3:1596-1607.
34. Muñoz L, Borrero MJ, Úbeda M, Conde E, Del Campo R, Rodríguez-Serrano M, Lario M, Sánchez-Díaz AM, Pastor O, Díaz D, García-Bermejo L, Monserrat J, Álvarez-Mon M, Albillos A. Intestinal Immune Dysregulation Driven by Dysbiosis Promotes Barrier Disruption and Bacterial Translocation in Rats With

Cirrhosis. Hepatology. 2019; 70:925-938.
35. Schneider KM, Mohs A, Gui W *et al*. Imbalanced gut microbiota fuels hepatocellular carcinoma development by shaping the hepatic inflammatory microenvironment. Nature Communications 2022; 13:3964.
36. Schuster S, Cabrera D, Arrese M, Feldstein AE. Triggering and resolution of inflammation in NASH. Nat Rev Gastroenterol Hepatol. 2018; 15:349-364.

Received April 18, 2024; Revised June 16, 2024; Accepted June 22, 2024.

[§]These authors contributed equally to this work.
**Address correspondence to:*
Yujun Shi and Yongjie Zhou, Institute of Clinical Pathology & Department of Pathology, Key Laboratory of Transplant Engineering and Immunology, NHC, West China Hospital, Sichuan University, Chengdu 610041, China.
E-mail: shiyujun@scu.edu.cn (YS); yongjiezhou@scu.edu.cn (YZ)

Released online in J-STAGE as advance publication June 26, 2024.